





## Theoretical and experimental investigations on Fe<sub>2</sub>P-type magnets: Effects of Si and Co substitution on physical and magnetic properties

Stephan Erdmann <sup>1</sup>, Halil İbrahim Sözen <sup>1,2</sup>, Francois Guillou <sup>3</sup>, Hargen Yibole,<sup>3</sup> and Thorsten Klüner <sup>1</sup>

<sup>1</sup>*Institute of Chemistry, Carl-von-Ossietzky University of Oldenburg, D-26129 Oldenburg, Germany*

<sup>2</sup>*Mercedes-Benz Turk A.S., Orhan Gazi Mahallesi, Mercedes Bulvarı No. 17/1, Esenyurt, Istanbul 34519, Turkey*

<sup>3</sup>*College of Physics and Electronic Information, Inner Mongolia Key Laboratory for Physics and Chemistry of Functional Materials, Inner Mongolia Normal University, Hohhot 010022, China*



(Received 7 June 2024; accepted 9 August 2024; published 3 September 2024)

Fe<sub>2</sub>P-based magnets are known for their significant magnetic properties, making them useful in various technological applications. The aim of this study was to investigate the effects of Si and Co substitution on the physical and magnetic properties of the Fe<sub>2</sub>P compounds. In order to have a systematic understanding we have performed combined *ab initio* calculations and a set of experiments. Particular emphasis was placed on the study of preferential substitution sites, lattice constants, magnetic moments, and the Curie temperature ( $T_C$ ), which was further explored by considering the exchange interaction energies  $J_{ij}$ . Satisfactory agreement was observed between theoretical calculations and the predicted phase transition from the hexagonal to the body-centered-orthorhombic (BCO) crystal structure as a function of temperature. Theoretical calculations reveal that the  $2c$  position is the preferred site for Si, while Co is expected to occupy the  $3f$  sites. Theoretical analysis of the magnetic moments shows an increase up to  $3.64 \mu_B/\text{f.u.}$  for  $x = 0.5$  Si, which agrees with the experimental values of  $3.16 \mu_B/\text{f.u.}$  Co substitution in Fe<sub>2-y</sub>Co<sub>y</sub>P<sub>0.84</sub>Si<sub>0.16</sub> and Fe<sub>2-y</sub>Co<sub>y</sub>P<sub>0.59</sub>Si<sub>0.41</sub> resulted in a decrease in magnetic moments and consequently in other magnetic properties. Focusing on the Curie temperature, three different trends were found depending on the Si concentration. A dependence of the  $3f$ - $3f$  intralayer exchange interaction energies on Si was proposed as the reason for the trends and deduced as the reason for an increase in  $T_C$  at low, no change in  $T_C$  at medium, and a decrease in  $T_C$  at high Si concentrations.

DOI: [10.1103/PhysRevMaterials.8.094401](https://doi.org/10.1103/PhysRevMaterials.8.094401)

### I. INTRODUCTION

In recent years, there has been a growing scientific interest in new, affordable, and hard magnetic materials, driven by developments in renewable energy and electric transportation [1–5]. The global market for permanent magnet materials is dominated by two types of magnetic compounds: ferrites and Nd<sub>2</sub>Fe<sub>14</sub>B magnets [6].

Although ferrites, such as BaFe<sub>12</sub>O<sub>19</sub> and SrFe<sub>12</sub>O<sub>19</sub>, are inexpensive to produce and contain noncritical elements, their performance is relatively poor. This renders them unsuitable for applications that require a high magnetization. In such instances, magnets comprising rare-earth (RE) and transition metal (TM) elements, such as Nd<sub>2</sub>Fe<sub>14</sub>B, are employed.

In these magnets, the TM elements provide high magnetization while the RE elements raise high anisotropy, which together produce a high-performance material. A significant drawback of RE-TM magnets is their high cost, which is largely attributable to the resource-critical nature of the majority of RE elements [7–9]. In order to achieve a Curie temperature ( $T_C$  of up to  $\sim 585$  K), it is necessary to modify the Nd<sub>2</sub>Fe<sub>14</sub>B magnet with critical heavy RE elements such as Dy or Tb [10].

The prevalence of ferrite and Nd<sub>2</sub>Fe<sub>14</sub>B on the global market has resulted in a significant performance gap. Consequently, there has been a substantial amount of research conducted into the development of a suitable permanent magnetic material to address this discrepancy [11]. Ideally, this

material should be free of RE elements and include no expensive or critical elements, such as platinum. These prerequisites make the RE-free Fe<sub>2</sub>P compound and materials deriving from it very promising, as they are mostly based on abundant and inexpensive iron. Furthermore, the Fe<sub>2</sub>P compound exhibits a high magnetization of  $\sim 3 \mu_B/\text{functional unit (f.u.)}$  and a high uniaxial anisotropy [12–15] due to its hexagonal crystal structure.

One disadvantage of this compound family is that its Curie temperature is relatively low, 214 K [12,14,16,17]. However, this can be easily improved. The layered stacking of weakly magnetic  $3f$  sites and stronger  $3g$  sites along the  $c$  axis leads to complex and entangled magnetic interactions. In order to achieve specific magnetic properties such as those required for permanent magnets a particularly subtle compounding strategy must be employed, utilizing metal (Co) and/or metalloid (Si) substitutions [11,13,18]. This study solely examines the impact of Si and Co on the Curie temperature and other physical and magnetic properties. While Si doping increases the distance between the different magnetic layers and therefore the  $3f$ - $3g$  interaction energies, Co doping is reported to enhance the weak  $3f$ - $3f$  interaction energies in the  $a$  and  $b$  directions [11].

In order to gain a comprehensive understanding of the design of Fe<sub>2</sub>P-based permanent magnets that are free of RE elements, it is essential to perform an atomistic investigation. To achieve this, the physical and intrinsic magnetic properties of the binary Fe<sub>2</sub>P compound, including lattice

constants, total magnetic moments, and Curie temperatures, have been calculated. Subsequently, the impact of Si substitution on ternary  $\text{Fe}_2\text{P}_{1-x}\text{Si}_x$  ( $0 \leq x \leq 0.5$ ) compounds is investigated. Furthermore, the effect of Co substitution into the Fe sites has been considered for the quaternary  $\text{Fe}_{2-y}\text{Co}_y\text{P}_{1-x}\text{Si}_x$  ( $x = 0.16$  and  $0.41$ ,  $0 \leq y \leq 1$ ) compounds.

It is, however, important to note that the substitution of Si and Co can lead to significant alterations to the stable crystal structure of the materials. It has been reported that at low temperatures for  $x \geq 0.1$ , a competing body-centered orthorhombic (BCO) phase appears [19,20]. Likewise, an increase in the Co content can result in the emergence of a competing  $\text{Co}_2\text{P}$  structure [18]. The presence of competing phases presents a significant change in the experimental synthesis of ternary and quaternary compounds with defined compositions.

The paper is organized as follows: Section II provides an explanation of the computational and experimental details concerning the different methods used for the calculations and experiments. Section III A compares *ab initio*-based stability calculations for the competing crystal structures with experimental results and the structure of the  $\text{Fe}_2\text{P}$  compound. Section III B explains the theoretical influence of Si substitution, while Sec. III C handles the Co substitution. In Sec. III D, the physical and intrinsic magnetic properties of the compound, including like lattice constants, magnetic moments, and maximum energy product are reported. In Sec. III E, the Curie temperature  $T_C$  and  $J_{ij}$  exchange interaction energies are discussed in detail as the final intrinsic magnetic property. Finally, in Sec. IV the paper concludes with remarks and discussions.

## II. COMPUTATIONAL AND EXPERIMENTAL DETAILS

### A. Computational details

All first-principles calculations were performed within the framework of spin-polarized density functional theory (DFT) using the Vienna *ab initio* Simulation Package (VASP) [21,22]. The projector augmented-wave method was employed as implemented in VASP. Exchange-correlation effects were treated within the generalized gradient approximation of Perdew-Burke-Ernzerhof [23]. The Brillouin zone was sampled with a  $k$ -point mesh described by a  $\Gamma$ -centered grid, with  $10 \times 10 \times 10$  meshes for supercells containing 36 atoms. The cutoff energy for the plane-wave basis used was 500 eV, and the width of the smearing parameter was 0.1 eV. The convergence criteria within the self-consistent field scheme are set to be  $10^{-5}$  eV for all considered alloys. The values of all these input parameters provide an energy convergence with an error equal to or smaller than 1 meV/atom.

In order to estimate  $T_C$ , the exchange interaction energies  $J_{ij}$  for the converged ferromagnetic (FM) states of the hexagonal structure have been calculated via the Liechtenstein method [24] employing the magnetic force theorem approach. In this approach the exchange energies are determined by calculations of total energy variations for small deviations of some magnetic moments from the ground state magnetic configuration. The magnetic couplings were calculated using density functional theory, following the Korringa-Kohn-Rostoker (KKR) [25,26] Greens's function

method, implemented in the AKAIKKR [27] code—also known as MACHIKANEYAMA—within the atomic sphere approximation incorporating the coherent potential approximation (CPA) [28,29]. The atomic sphere radii are based on the Wigner-Seitz radii of each atom. Continuous concentration changes for both the Fe and P sublattices are considered based on KKR-CPA. All KKR calculations are based on the local density approximation [30,31], taking the exchange-correlation function as parametrized by Moruzzi, Janak, and Williams [32]. In this work, the scattering is considered up to  $d$  scattering ( $l_{\max} = 2$ ) in the systems. For the Brillouin zone quality 448  $k$  points in the irreducible Brillouin zone were chosen together with an edelt value of 0.001 Ry to achieve a convergence of the Curie temperatures up to a variation of only 5 K. As an input structure for each KKR calculation, the theoretically relaxed (VASP, GGA-PBE) and experimentally found values are considered.

### B. Experimental details

A new batch of  $\text{Fe}_{1.93}\text{P}_{1-x}\text{Si}_x$  ternary compounds with  $x = 0, 0.05, 0.10, 0.15, 0.20, 0.25, 0.30, 0.35, 0.40, 0.4, 0.5,$  and  $0.6$  was prepared by ball milling elemental starting materials during 10 h, followed by a solid-state reaction. The samples were shaped by uniaxial pressing at 750 MPa into cylinders of approximately 2.5 g and sealed in quartz tubes backfilled with 200 mbar Ar gas. The sintering is carried out at 1100 °C for 24 h ending by a quenching in room temperature water. Powder x-ray diffraction experiments were carried out at room temperature. This new dataset is found in line with the phase diagram reported in [33]. Structural refinements indicate that  $x \leq 0.20$  samples crystallize in the  $\text{Fe}_2\text{P}$  crystal structure at room temperature. From  $0.25 \leq x \leq 0.4$ , the samples crystallize in the BCO structure. Despite using off-stoichiometric nominal compositions, secondary phases having a 3:1 metal:metalloid ratio are found in most samples. The secondary phase content progressively increases with Si substitutions from about 4 wt % of tetragonal  $\text{Fe}_3\text{P}$  secondary phase in the  $x = 0.05$  sample, up to about 9 wt % of cubic  $\text{Fe}_3\text{Si}$  in the  $x = 0.40$  sample. For  $x = 0.5$ , the main phase still presents a BCO structure ( $\sim 70$  wt.%), but particularly large amounts of  $\text{Fe}_3\text{Si}$  and  $\text{Fe}_5(\text{P}, \text{Si})_3$  secondary phases are observed. Magnetization measurements were carried out using the vibrating sample magnetometer option of a Quantum Design Versalab system on oriented powders. Oriented polycrystalline samples were prepared by pulverizing bulk pieces, sieving the powder below 20  $\mu\text{m}$  and orienting them into an external field of 11 kOe while using epoxy as a binder.

## III. RESULTS AND DISCUSSION

### A. Phase stabilities of the $\text{Fe}_2\text{P}_{1-x}\text{Si}_x$ compounds

The schematic representation of the hexagonally structured compound is depicted in Fig. 1. The primitive cell is composed of six Fe and three P atoms. The Fe atoms are distributed evenly across the  $3f$  and  $3g$  sites, while the P atoms are located in the  $1b$  and  $2c$  sites with a ratio of 1:2. The  $3f$  iron atoms are located in a tetrahedral environment formed by two metalloids in the  $2c$  positions and two metalloids in the  $1b$  positions. The  $3g$  sites are surrounded by four metalloids

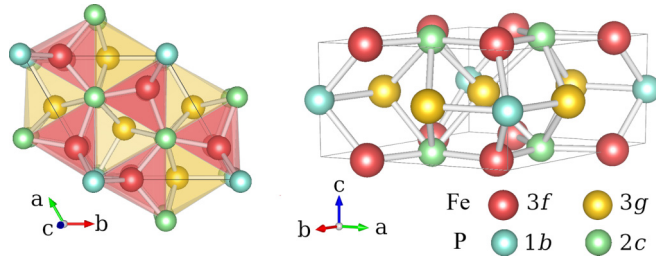


FIG. 1. Schematic representation of the substitution-free hexagonal  $\text{Fe}_2\text{P}$ -primitive cell with the different Fe and P sites shown.

in the  $2c$  positions and one metalloid in the  $1b$  positions forming a square-based pyramid.

It can be seen that the  $3f$  and  $3g$  sites are stacked in layers along the  $c$  axis. The  $\text{Fe}_2\text{P}$  parent compound is known to accommodate various substitution schemes. The iron in the  $3f$  or  $3g$  sites may be substituted by a broad range of  $3d$  (Ti to Ni) or  $4d$  (Nb, Ru, Rh, Pd) metals, while the phosphorous may be substituted by other metalloids or poor metals such as B, Si, Ge, or As. Nevertheless, such substitutions rapidly challenge the stability of the desired hexagonal crystal structure of  $\text{Fe}_2\text{P}$ .

In the case of Si for P substitutions, experimental studies have demonstrated that a phase transition occurs at room temperature for  $\text{Fe}_2\text{P}_{1-x}\text{Si}_x$  between  $0.2 \leq x \leq 0.25$  Si per f.u., whereby the hexagonal phase transforms into a (BCO) phase. The BCO phase represents a slight deformation of the hexagonal structure, resulting in the breaking of the alignment of the  $3f$  and  $3g$  sites originally observed along the  $c$  direction of the  $\text{Fe}_2\text{P}$  structure. At higher Si contents ( $x \geq 0.5$ ), a significant increase in the amount of secondary phases is observed in the samples, which coincides with the emergence of a mixed-phase region where the BCO structure coexists with substantial quantities of cubic  $\text{Fe}_3\text{Si}$ -type and hexagonal  $\text{Fe}_5\text{Si}_3$ -type phases.

Figure 2 presents the formation energy for the different structures as a function of the Si substitution in  $\text{Fe}_2\text{P}_{1-x}\text{Si}_x$  ternary compounds. The experimental phase transitions at room temperature are indicated by changes in the background color from red (hexagonal) to blue (BCO) to gray (mixed phase) [33]. Furthermore, the extrapolation to low temperatures of the temperature dependence of the phase transition from  $\text{Fe}_2\text{P}$ -type to BCO is marked with a vertical dashed line (at  $x \approx 0.1$ ) [19,20]. In order to provide a comprehensive analysis, the stability of the end member of the series, the binary  $\text{Fe}_2\text{Si}$  having a trigonal structure, has been included in the formation energy calculations. The formation energies  $E_{\text{form}}$  in Fig. 2 are calculated using the following equation with the energies of the reference elements (bcc ferromagnetic Fe, triclinic nonmagnetic P, and fcc nonmagnetic Si):

$$E_{\text{form,un}} = E(\text{Fe}_2\text{P}_{1-x}\text{Si}_x) - 2E(\text{Fe}) - xE(\text{Si}) - (1-x)E(\text{P}). \quad (1)$$

In our DFT calculations, the transition to the BCO structure occurs at  $x \approx 0.08$ – $0.1$  Si per f.u., where the formation energy of the BCO phase is slightly lower than that of the hexagonal structure. At  $x \approx 0.6$  Si per f.u., the formation energies of the

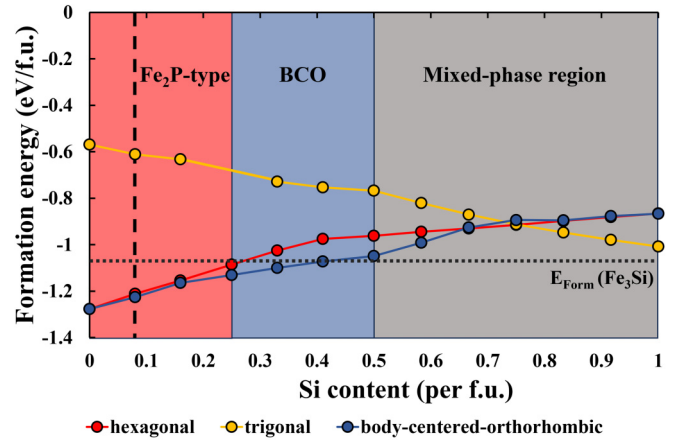


FIG. 2. Comparison of the calculated formation energies for the ternary  $\text{Fe}_2\text{P}_{1-x}\text{Si}_x$  compound in the hexagonal, trigonal, and body-centered orthorhombic (BCO) structures. The colored backgrounds indicate the experimentally observed transitions at room temperature by Bao *et al.* [33] while the dashed line shows the experimentally found transition to BCO at low temperature by Severin *et al.* [20]. The horizontal dotted line indicates the calculated formation energy of  $(\text{Fe}_3\text{Si})$  considering unary elements [see Eq. (1)].

trigonal, BCO, and hexagonal structures are comparable. This corresponds to the substitution range where a mixed-phase region is experimentally observed.

A comparison of the results in the figure with the 0 K DFT calculations reveals a very satisfactory agreement. The calculated  $\text{Fe}_2\text{P}$ -type to BCO structure change between 0.08 and 0.1 Si per f.u. is in accordance with the experimental  $x \approx 0.1$ . Experimentally, the hexagonal to BCO transition has been found to be also induced by the temperature [19,20]. The temperature of the structural transition exhibits a dependence on the Si content, with the structural transition temperature increasing with the Si content until  $x = 0.3$ . Consequently, at room temperature, the transition is observed near  $\text{Si} \approx 0.2$ . The present theoretical results indicate a modest (yet growing) difference in formation energy between hexagonal and BCO structures in the Si range 0.1–0.2, which is consistent with the experimental observations.

The calculated formation energy for  $\text{Fe}_3\text{Si}$  of  $-1.08$  eV/f.u. provides further support for the experimental transition into the mixed-phase region, with  $\text{Fe}_3\text{Si}$  being identified as the dominant phase for  $x \geq 0.5$ . This is due to the lower formation energy of  $\text{Fe}_3\text{Si}$  compared to the BCO and hexagonal structures. This work further investigates the hexagonal structure due to its stability at higher temperatures and the associated magnetic properties.

## B. Si substitution

It is reported that chemical substitution in  $\text{Fe}_2\text{P}$  favors the development of a site preference in the various nonequivalent positions. In general, for metallic  $3f$  and  $3g$  sites, elements lighter than Fe (e.g., Mn or Cr) will preferentially occupy the pyramidal  $3g$  site, while heavier elements (Co or Ni) will preferentially substitute the tetrahedral  $3f$  site. With regard to the metalloid sites, it appears that selectivity based on a size criterion occurs with large metalloids (such as Ge or As)

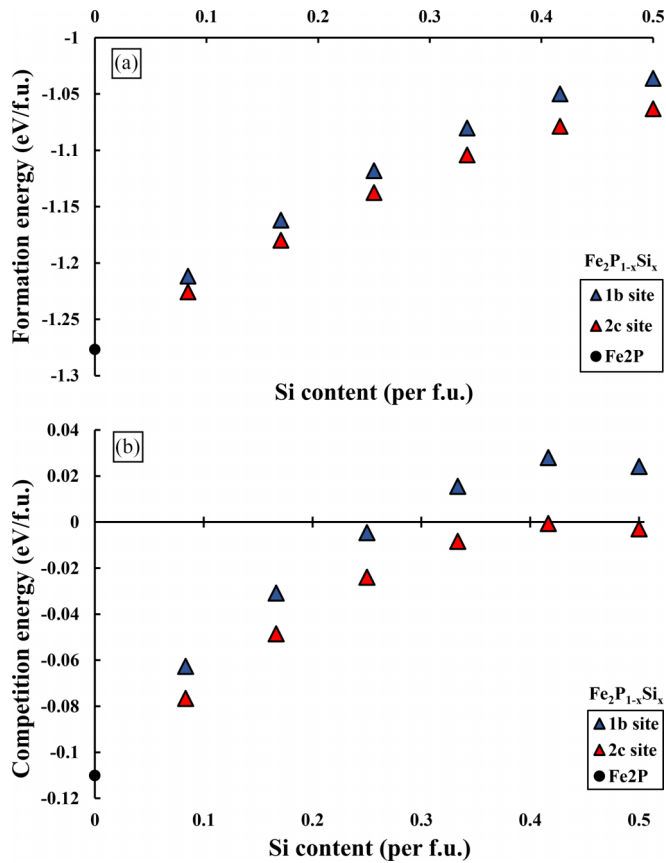


FIG. 3. (a) Formation energy for the substitution of Si into the  $1b$  and  $2c$  sites of the  $\text{Fe}_2\text{P}_{1-x}\text{Si}_x$  compound calculated directly with the energy of the elements bcc ferromagnetic Fe, triclinic nonmagnetic P, and fcc nonmagnetic Si [see Eq. (1)]. (b) Calculation of the competition energy for the substitution of Si into the  $1b$  and  $2c$  sites of the  $\text{Fe}_2\text{P}$  compound considering the energy of the binary compounds FeP and FeSi as well as bcc ferromagnetic Fe [see Eq. (2)].

occupying preferentially the largest  $2c$  site while elements smaller than P will preferentially sit in the smaller  $1b$  site (B or C) [34–37]. Consequently, it can be postulated that Si substitution will result in a site preference for the larger  $2c$  site given that Si is slightly larger than P [38]. Figure 3 illustrates the calculated formation and competition energies for the  $1b$  and  $2c$  sites, presented for two distinct calculation methodologies up to  $x = 0.5$  Si per f.u. The formation energies  $E_{\text{form}}$  are calculated using Eq. (1) while the following equation is used to calculate binary competition energies  $E_{\text{comp}}$ :

$$E_{\text{comp,bin}} = E(\text{Fe}_2\text{P}_{1-x}\text{Si}_x) - 1E(\text{Fe}) - xE(\text{FeSi}) - (1-x)E(\text{FeP}). \quad (2)$$

In Fig. 3(a) the formation energy is calculated with the energies of the reference elements as mentioned before, while in Fig. 3(b) the energies of the energetically most stable Fe-P and Fe-Si binary compounds (FeP and FeSi [39,40]) and bcc Fe are considered [as given in Eq. (2)]. In both cases, the energy for the  $2c$  site is lower than that of the  $1b$  site, indicating a preference for the  $2c$  site (in accordance with the selectivity based on a size criterion for the metalloids). This result is

consistent with previous theoretical investigations that have identified Si substitutions into the  $2c$  site as more favorable than those into the  $1b$  site [41–43].

At low Si content, the difference between the two sites is minimal, but it becomes more pronounced with higher Si concentrations. Furthermore, a higher Si content also leads to higher energies and, therefore, lower stability. It should be noted that, with an increase in Si content, the slope of the energy increase becomes less pronounced and appears to reach a peak at approximately 0.4 Si per f.u. A direct comparison of Figs. 3(a) and 3(b) also demonstrate that, when considering stable binary compounds, the energy is significantly higher and even yields positive values beyond  $\sim 0.3$  Si per f.u., meaning high Si containing ternaries are unlikely to form. This results in a solubility limit of Si in  $\text{Fe}_2\text{P}$  compounds of 10–13 at. %.

With regard to the Si site occupancy, it is important to recall that controversies can arise in the context of preferential substitutions in the metalloid  $2c$  and  $1b$  sites. In the case of the ternary  $\text{Fe}_2(\text{P,As})$  compound, an analysis of the x-ray diffraction intensities indicated that As atoms preferentially occupy the  $2c$  site [44]. However, a neutron diffraction study of closely related  $\text{MnFe}(\text{P,As})$  quaternary compounds with a  $\text{Fe}_2\text{P}$  structure did not conclude on a preferential P/As selectivity [36] and random P/As substitution was also supported by Mössbauer spectroscopy [45]. In the case of substitutions of P by smaller B, a preferential site occupancy of B in the  $1c$  site was observed in ternary  $\text{Fe}_2(\text{P,B})$  from Mössbauer spectroscopy [46] and from neutron diffraction in pseudo-quaternary  $(\text{Mn, Fe})_2(\text{P,Si,B})$  compounds [47].

The case of Si for P substitutions can be anticipated to be even more challenging due to the limited size difference. In ternary  $\text{Fe}(\text{P,Si})$  compounds, a former theoretical investigation predicted a preferential site occupancy of Si for the largest  $2c$  site [48]. However, no preferential ordering could be resolved experimentally from Mössbauer spectroscopy [19]. In the quaternary  $(\text{Mn, Fe})_2(\text{P,Si})$  compound, a random P/Si occupation was observed up to  $\text{Si} = 0.4$  from neutron diffraction, while a preferential occupancy of Si for the  $2c$  site was experimentally observed only at the highest Si contents,  $0.42 \leq \text{Si} \leq 0.55$  [35].

Our formation and competition energy calculations systematically indicate a preferential occupation of Si in  $2c$  sites. However, it is noteworthy that the differences in the energies between  $2c$  and  $1b$  occupation are relatively modest, amounting to approximately 0.01 eV/f.u. at low Si concentrations. Such small energy differences corresponding to only a few hundred K could potentially be overcome at the synthesis stage, involving a solid-state reaction at 1373 K. Consequently, it remains possible that a significant Si preferential occupation in the  $2c$  sites will develop in  $\text{Fe}_2\text{P}_{1-x}\text{Si}_x$  compounds only at large Si substitutions, showing larger energy differences.

### C. Co substitution

The substitution of Si into the  $\text{Fe}_2\text{P}$  compound leads to the emergence of the competing BCO structure. Bao *et al.* [33] investigated the influence of Co substitution at Fe sites on various phase transitions, reporting that Co substitution expands

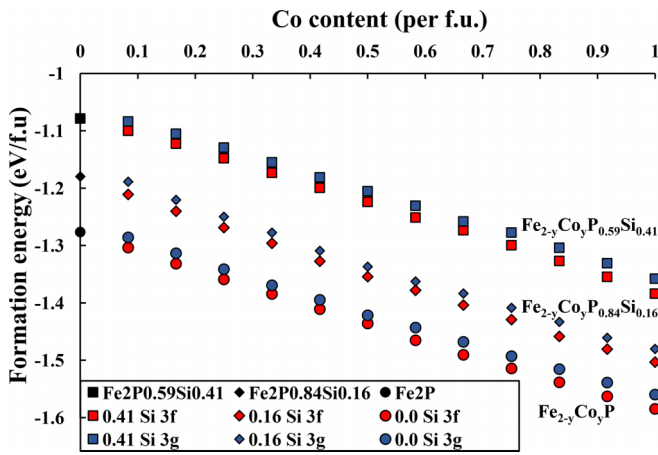


FIG. 4. Formation energy (calculated from unaries) for quaternary compounds in dependence of Co substitution into the 3f and 3g sites in the  $\text{Fe}_2\text{P}$ ,  $\text{Fe}_2\text{P}_{0.84}\text{Si}_{0.16}$ , and  $\text{Fe}_2\text{P}_{0.59}\text{Si}_{0.41}$  compounds.

the range of the hexagonal phase and modifies the magnetic properties. However, high Co content induces a phase transition to the  $\text{Co}_2\text{P}$  structure.

Literature suggests that metal site substitution (3f and 3g) depends on the number of  $d$  electrons, with elements possessing fewer  $d$  electrons preferentially occupying the pyramidal Fe site (3g site in  $\text{Fe}_2\text{P}$ ) [34]. This is supported by Bacmann *et al.* [36] and Dung *et al.* [37], who observed a strong preference for Mn substitution at the 3g site in  $(\text{Fe}, \text{Mn})\text{P}_{1-x}\text{As}_x$  and  $(\text{Fe}, \text{Mn})\text{P}_{1-x}\text{Si}_x$  compounds. For Co, this implies a preferred substitution at the tetrahedron 3f site in  $\text{Fe}_2\text{P}$ , as confirmed by neutron diffraction experiments in  $(\text{Fe}, \text{Co})_2\text{P}$  ternary compounds [49] and by Zhuralev *et al.* [42].

In this work, the substitution of Co into the 3f and 3g sites for  $\text{Fe}_{2-y}\text{Co}_y\text{P}_{1-x}\text{Si}_x$  compounds with Si-free ( $x = 0$ ), low Si ( $x = 0.16$ ), and a high Si content ( $x = 0.41$ ) was considered. Figure 4 presents the theoretical results for all three cases. The formation energy was calculated using the ground state energies of reference elements [Eq. (1)]. As shown in Fig. 3, Co substitution follows a trend of increasing formation energy with higher Si concentrations, with the unsubstituted  $\text{Fe}_2\text{P}$  compound having the lowest formation energy at 1.27 eV/f.u.

Unlike Si substitution, Co substitution results in a steady decrease in energy with increasing Co content. Comparing the 3f (red) and 3g (blue) substitution sites, the 3f is consistently preferred, with an energy difference of  $\sim 0.02$  eV/f.u. across all cases. This indicates that the Si substitution does not influence the site preference for Co substitution, as the 3f site remains energetically favored.

#### D. Physical and magnetic properties

As  $(\text{Fe}, \text{Co})_2(\text{P}, \text{Si})$  compounds are postulated to be promising RE-free magnetic materials, we investigate their physical and magnetic properties, including the lattice constants and the total magnetic moment. Emphasis is placed on the lattice constants  $a$  and  $c$ , as well as the  $c/a$  ratio, due to their significant influence on the  $T_C$ . Given the differing atomic sizes of Si and P, Si substitution for P is expected to cause overall volume expansion, while Co substitution for Fe results in volume

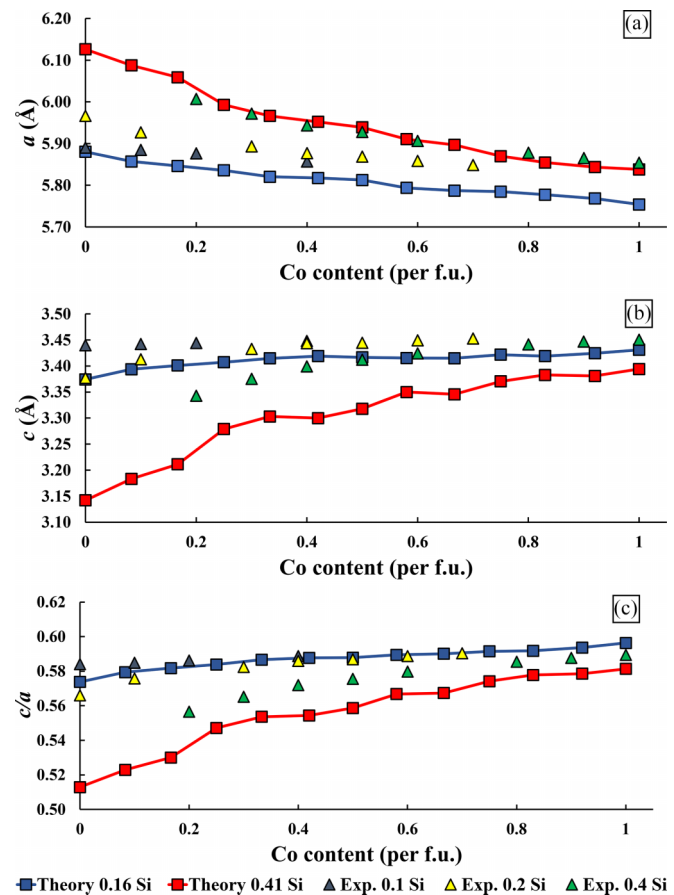


FIG. 5. Lattice constants  $a$  (a) and  $c$  (b) and  $c/a$  ratio (c) in dependence on Co content. Theoretical investigations for 0.16 and 0.41 Si per f.u. are displayed as squares and experimental results for 0.1, 0.2, 0.4, and 0.5 Si per f.u. as triangles.

contraction. These structural changes are often anisotropic in the hexagonal structure, necessitating investigation of each axis.

Figure 5 shows theoretical calculations of the lattice constants  $a$  and  $c$ , as well as the  $c/a$  ratio for  $\text{Fe}_{2-y}\text{Co}_y\text{P}_{1-x}\text{Si}_x$  compounds in the hexagonal crystal structure with  $x = 0.16$  and 0.41 Si per f.u. For comparison, experimental data for  $x = 0.1, 0.2, 0.4$  Si per f.u. are also presented [33].

The substitution of Si for P increases the lattice parameter  $a$  from  $\approx 5.88$  Å to  $\approx 6.12$  Å for 0.16 to 0.41 Si per f.u., whereas substituting Co for Fe systematically decreases  $a$  down to 5.77 and 5.85 Å, respectively, for  $\text{Co} = 1$ . Conversely, the  $c$  axis exhibits opposite trends: Si substitutions reduce  $c$  from  $\approx 3.38$  to  $\approx 3.15$  Å, while Co substitution increases it to about 3.40 and 3.37 Å for  $\text{Co} = 1$ . As a result the  $c/a$  ratio shows significant changes. For the Si = 0.16 compound, the  $c/a$  increases from  $\approx 0.57$  up to  $\approx 0.59$  with Co substitutions. For the Si = 0.41 Si compound, the ratio increases from 0.51 to 0.57 for  $y = 0$  to 1.0 Co per f.u. Similar trends for the change of the lattice constants with Si have been reported for  $(\text{Fe}, \text{Mn})_2(\text{P}, \text{Si})$  compounds [50].

The DFT-calculated lattice parameters and their evolution align well with experimental and theoretical literature [11,33,41,48,51]. Notably, a discrepancy is observed in

the lattice parameters reported by Bao *et al.* [33], where theoretical values are underestimated at 0.16 Si per f.u. but nearly identical at 0.41 Si per f.u. The difference is reasonable, considering the limitations of each approach. As a result of the size limitations of the supercell to achieve the correct composition of the compounds, the evolution of the lattice constants can deviate from a perfect linear trend. Experimental values were obtained from polycrystalline samples based on off-stoichiometric nominal compositions and containing noticeable amounts of secondary phase, while DFT calculations reflect a ground state structure compared to room temperature experimental parameters. Understanding the structure of  $(\text{Fe, Co})_2(\text{P,Si})$  compounds and its evolution with substitution rates is crucial for subsequent magnetic investigations.

### E. Total magnetic moments

One of the most crucial magnetic properties of the compounds is their magnetization. In this work, results are presented in terms of magnetic moment and saturation magnetization  $J_S$ , expressed as  $\mu_0 M_S$ . The total magnetic moment, given in Bohr magnetons ( $\mu_B$ ) per formula unit (f.u.), represents the cumulative sum of the magnetic moments of the individual atoms. The saturation magnetization is expressed in Tesla (T), is calculated using the compound density ( $\rho$ ), the Avogadro constant ( $N_A$ ), the molecular weight ( $M_{\text{alloy}}$ ), and the average magnetic moment per atom ( $m_{\text{atom}}^{\text{tot}}$ ):

$$\mu_0 M_S = m_{\text{atom}}^{\text{tot}} \mu_B \frac{\rho N_A}{M_{\text{alloy}}}. \quad (3)$$

The calculated results for the total magnetic moment and the contribution of the 3*f* and 3*g* sites dependent on Si and Co substitution are shown in Fig. 6. In this work, only the ferromagnetic configuration has been considered for the investigated compounds.

The total magnetic moments for the parent  $\text{Fe}_2\text{P}$  compound was found to be  $3.02 \mu_B/\text{f.u.}$ , which is in reasonable agreement with the  $2.94 \mu_B/\text{f.u.}$  reported for a fully saturated  $\text{Fe}_2\text{P}$  single crystal measured with the applied magnetic field oriented along its easy magnetocrystalline anisotropy direction [12]. Theoretical values of  $3.08$  and  $2.94 \mu_B/\text{f.u.}$  reported by Liu *et al.* and Eriksson *et al.*, respectively, also align well with these experimental results [52,53]. Our calculations indicate that substituting Si for P progressively increases the total magnetic moment, reaching up to  $3.64 \mu_B/\text{f.u.}$  for  $x = 0.5$  Si per f.u., compared to  $3.02 \mu_B/\text{f.u.}$  for the substitution-free case. This increase is primarily due to higher magnetic moments of Fe atoms in the 3*f* position, consistent with previous theoretical works [48,54,55]. A similar influence of Si was reported for  $(\text{Fe, Mn})_2(\text{P,Si})$  compounds, where the magnetic moment rises with the Si content as well [48]. The magnetic moment of the 3*f* site increases from a value of  $\approx 0.8 \mu_B/\text{f.u.}$  at  $x = 0$  to  $1.5 \mu_B/\text{f.u.}$ , while the 3*g* site moments remain at  $\approx 2.2 \mu_B/\text{f.u.}$

This trend of a general increase in magnetic moments with Si for P substitutions is also observed on the experimental magnetic moments. Total magnetic moments of  $\text{Fe}_{1.93}\text{P}_{1-x}\text{Si}_x$  powders, measured at  $T = 50$  K and  $\mu_0 H = 3$  T, significantly increase from  $x = 0$  to 0.2, though no clear trend is observed for BCO structure samples from  $x = 0.25$  to 0.5. It

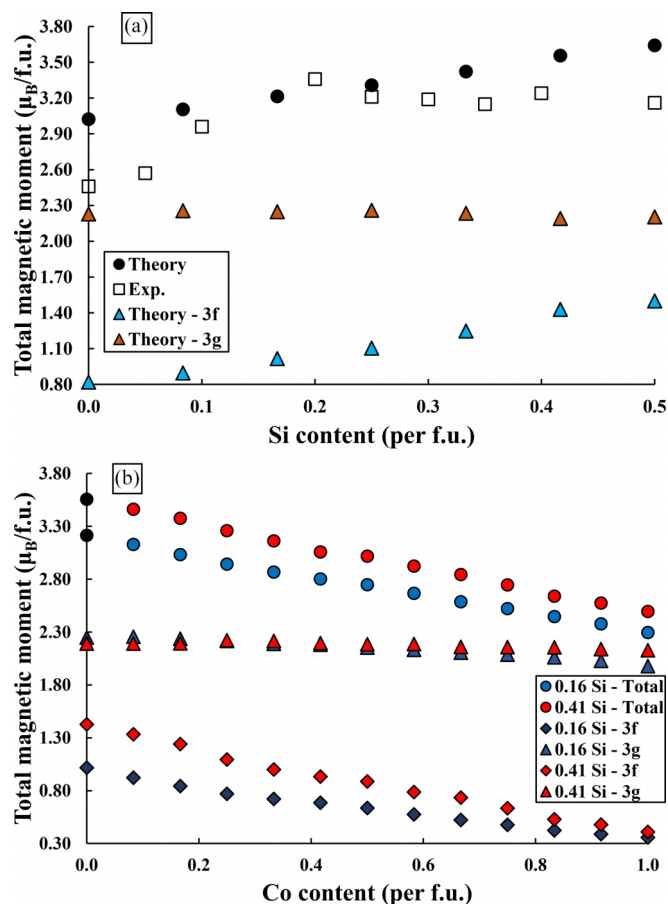


FIG. 6. (a) Total magnetic moments (full circles) for the substitution of Si into the hexagonal  $\text{Fe}_2\text{P}_{1-x}\text{Si}_x$  compound up to 0.5 Si per f.u. with the contributions of the 3*f* (blue) and 3*g* (red) sites as triangles. Experimental values are shown as empty squares. (b) Total magnetic moment for the substitution of Co into the hexagonal  $\text{Fe}_{2-y}\text{Co}_y\text{P}_{1-x}\text{Si}_x$  compounds for  $x = 0.16$  (blue) and 0.41 Si per f.u. (red) with the contribution of the 3*f* (diamonds) and the 3*g* (triangles) sites shown.

should be noted, that the experimental results are subject to some uncertainties since (i) non-negligible secondary phases are present in the samples and (ii) the experimental conditions do not allow for a complete saturation. Nevertheless, the experimental results are consistent with the theoretical increase in magnetization observed with Si substitution for P.

As the saturation polarizations ( $J_S$ ) are calculated based on the magnetic moments, a same trend is observed. The calculated  $J_S$  values for Si substitutions in  $\text{Fe}_2\text{P}_{1-x}\text{Si}_x$  ternary compounds are listed in Table I. The increase in total magnetic moments significantly exceeds the unit cell expansion, predicting a substantial increase in saturation polarization due to Si for P substitutions. We note that saturation polarizations larger than 1 T are well compatible and actually desired for permanent magnets, confirming that Si for P substitutions will be beneficial for applications.

In the case of Co substitution, an opposing effect to Si is observed. At low Co concentrations, the total magnetic moment for  $x = 0.16$  Si and 0.41 Si are  $3.21$  and  $3.56 \mu_B/\text{f.u.}$ , respectively. These values decrease with an increasing Co

TABLE I. Theoretical magnetic moments and saturation polarizations for hexagonal  $\text{Fe}_2\text{P}_{1-x}\text{Si}_x$  compounds.

$x$	$M$ ( $\mu_B/\text{f.u.}$ )	$J_S$ theory (T)
0.00	3.02	1.06
0.08	3.11	1.08
0.16	3.21	1.11
0.25	3.31	1.14
0.33	3.42	1.17
0.41	3.56	1.22
0.50	3.64	1.24

concentration, reaching a minimum of 2.30 and 2.49  $\mu_B/\text{f.u.}$  for a complete substitution of the  $3f$  Fe sites ( $y = 1.0$  Co per f.u.). This decrease is linked to the magnetic moment of the  $3f$  site, where the Co substitution occurs, reducing from 0.92 and 1.33  $\mu_B/\text{f.u.}$  to only 0.36 and 0.41  $\mu_B/\text{f.u.}$  at  $y = 1$  Co per f.u. The magnetic moment of the Fe  $3g$  atoms remains largely unperturbed by the substitution, with minor changes observed only in the 0.16 Si compound. Here, a slight decrease from 2.26  $\mu_B/\text{f.u.}$  at  $y = 0$  Co down to 1.98  $\mu_B/\text{f.u.}$  at 1.0 Co per f.u. occurs. The effect is considerably less pronounced for 0.41 Si, with the value changing by only 0.07  $\mu_B/\text{f.u.}$  from 2.19 to 2.12  $\mu_B/\text{f.u.}$  The predicted decrease of the total magnetic moments due to Co substitutions aligns with experimental observations, which report a reduction in saturation polarization with the increase in Co concentration for  $\text{Fe}_{2-y}\text{Co}_y\text{P}_{1-x}\text{Si}_x$  polycrystalline samples and single crystals [11,33,56,57]. This trend is further corroborated by Zhuralev *et al.* [42], who also found a decrease of the magnetic moments with increasing Co content.

#### F. Maximum energy product $|BH|_{\max}$

In the case of an ideal hysteresis loop, there is a direct relationship between the  $|BH|_{\max}$  and  $M_S$ , as in this case  $M_r$  is maximum and  $\mu_0 M_r = \mu_0 M_S$  is given. Thus, the theoretical calculation of  $|BH|_{\max}$  is as follows [58,59]:

$$|BH|_{\max} = \frac{\mu_0 M_S^2}{4}, \quad (4)$$

where  $\mu_0$  is the vacuum permeability ( $\mu_0 = 4\pi \times 10^{-7} \text{N A}^{-2}$ ). The calculated  $|BH|_{\max}$  values are shown in Table II.

Inherent to its definition, the theoretical  $|BH|_{\max}$  follows the same trends found for the magnetization. With Si the  $|BH|_{\max}$  of 222.3  $\text{kJ/m}^3$  of the unsubstituted  $\text{Fe}_2\text{P}$  compound increases to 245.7 and 295.5  $\text{kJ/m}^3$  for  $x = 0.16$  and 0.41 Si per f.u., respectively. This trend of an increase was also reported by He *et al.* [11] who described a steady improvement of the  $|BH|_{\max}$  from 141  $\text{kJ/m}^3$  for  $(\text{Fe}_{0.91}\text{Co}_{0.09})_2(\text{P}_{0.89}\text{Si}_{0.11})$  up to 204  $\text{kJ/m}^3$  for  $(\text{Fe}_{0.91}\text{Co}_{0.09})_2(\text{P}_{0.74}\text{Si}_{0.26})$ . With a steady raise of the amount of Co, the  $|BH|_{\max}$  decreases for both investigated compounds down to values of 132.4  $\text{kJ/m}^3$  ( $x = 0.16$  Si) and 150.8  $\text{kJ/m}^3$  ( $x = 0.41$  Si).

TABLE II. Calculated  $|BH|_{\max}$  values for quaternary  $\text{Fe}_{2-y}\text{Co}_y\text{P}_{1-x}\text{Si}_x$  compounds with  $y = 0.16$  and 0.41.

Compound	$ BH _{\max}$ ( $\text{kJ/m}^3$ )	$ BH _{\max}$ ( $\text{kJ/m}^3$ )
	$x = 0.16$	$x = 0.16$
$\text{Fe}_2\text{P}_{1-x}\text{Si}_x$	245.7	295.5
$\text{Fe}_{1.92}\text{Co}_{0.08}\text{P}_{1-x}\text{Si}_x$	233.8	280.2
$\text{Fe}_{1.84}\text{Co}_{0.16}\text{P}_{1-x}\text{Si}_x$	220.9	266.4
$\text{Fe}_{1.75}\text{Co}_{0.25}\text{P}_{1-x}\text{Si}_x$	208.2	248.3
$\text{Fe}_{1.67}\text{Co}_{0.33}\text{P}_{1-x}\text{Si}_x$	198.6	234.4
$\text{Fe}_{1.59}\text{Co}_{0.41}\text{P}_{1-x}\text{Si}_x$	190.5	219.9
$\text{Fe}_{1.50}\text{Co}_{0.50}\text{P}_{1-x}\text{Si}_x$	184.8	215.6
$\text{Fe}_{1.42}\text{Co}_{0.58}\text{P}_{1-x}\text{Si}_x$	174.7	202.2
$\text{Fe}_{1.33}\text{Co}_{0.67}\text{P}_{1-x}\text{Si}_x$	165.3	193.7
$\text{Fe}_{1.25}\text{Co}_{0.75}\text{P}_{1-x}\text{Si}_x$	156.6	180.7
$\text{Fe}_{1.16}\text{Co}_{0.84}\text{P}_{1-x}\text{Si}_x$	148.7	167.4
$\text{Fe}_{1.08}\text{Co}_{0.92}\text{P}_{1-x}\text{Si}_x$	140.9	160.7
$\text{Fe}_{1.0}\text{Co}_{1.0}\text{P}_{1-x}\text{Si}_x$	132.4	150.8

#### G. Curie temperature

$\text{Fe}_2\text{P}$  is well known for its relatively low Curie temperature ( $T_C$ ) of 214 K, which poses a limitation to its applicability in certain magnetic applications [12,14,16,17]. To address this limitation, the substitution of Fe and P with other elements has been explored as a means to significantly enhance  $T_C$  [11,33,41]. Similar strategies have proven effective in analogous compounds incorporating elements such as Co and Si [36,37,43,44,60,61].

To determine the theoretical  $T_C$  values, an effective spin Heisenberg model is adopted and solved in the mean-field approximation (MFA). In this Heisenberg model the Hamiltonian of the spin-spin interaction is given by  $H = \sum_{i \neq j} J_{ij} \vec{S}_i \vec{S}_j$ , where  $\vec{S}_i$  and  $\vec{S}_j$  correspond to the spin of place  $i$  and  $j$ , respectively.  $J_{ij}$  corresponds to the exchange coupling constant between the two sites  $i$  and  $j$  and was calculated with AKAIKKR [27]. The absolute value of the magnetic ordering temperature  $T_C$  resulting from MFA is  $k_B T_C = \frac{3}{2} J_0$ , where  $k_B$  is the Boltzmann constant and  $J_0$  is the sum of  $J_{ij}$ . Therefore,  $J_0$  is the total effective exchange of a given lattice site connected to all others. The main drawback of the evaluation of  $J_{ij}$  when considering the FM configuration, is the systematic overestimation of  $T_C$  ( $\sim 45\%$ ). Note, that this overestimation is the result of some limitations of the KKR-CPA method, as it fails to include correlation effects, short-range ordering, electron-electron interactions, and multiple scattering effects [62–64]. Nonetheless, even with these limitations the KKR-CPA calculations are precise enough to capture the possible trends in the Curie temperatures.

In this study, the impact of Co and Si substitution on the  $T_C$  of  $\text{Fe}_{2-y}\text{Co}_y\text{P}_{1-x}\text{Si}_x$  compounds has been examined and the experimental lattice constants from Bao *et al.* [33] have been employed as input for better comparability. With theoretically relaxed lattice constants the same trends for  $T_C$  were found as described for the experimental ones. Our findings, presented in Fig. 7, are accompanied by experimental results from Bao *et al.* for comparison. As illustrated, the calculated FM ground state approximation consistently exceeds the experimental values, as anticipated.

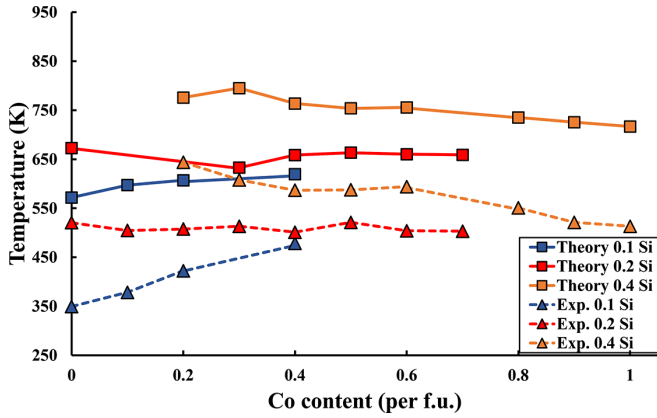


FIG. 7. Experimental (dashed lines with triangles) and theoretical (solid lines with squares) results for the Curie temperature  $T_C$  for  $\text{Fe}_{2-y}\text{Co}_y\text{P}_{1-x}\text{Si}_x$  with  $x = 0.1, 0.2,$  and  $0.4$  Si per f.u.

As the Si content increases, a notable rise in  $T_C$  is observed, going up from 214 K with no Si to  $\approx 350$  K for 0.1 Si per f.u. and  $\approx 520$  K for 0.2 Si per f.u. This enhancement is corroborated by experimental reports [11,33,41] and similar to the influence of Si substitution on the  $T_C$  of  $(\text{Fe}, \text{Mn})_2(\text{P}, \text{Si})$  compounds [50]. However, further increments in Si content continue to augment  $T_C$  while introducing the competing BCO and  $\text{Co}_2\text{P}$  crystal structures, as previously discussed. The trend of an increasing  $T_C$  with Si substitutions is accurately mirrored in the theoretical calculations of this work, yielding values of  $\approx 570$  K for 0.1 Si and  $\approx 670$  K for 0.2 Si. Additionally, Zhuralev *et al.* [42] also reported theoretical  $T_C$  values in the order of  $\sim 700$  K determined by mean-field approximation.

Regarding Co, three distinct trends in dependence on the substituted amount of Si were identified, both for experimental and for theoretical results (see Fig. 7). At low Si content, both the experimental and the theoretical findings indicate an elevation in  $T_C$  with increasing Co up to  $\approx 480$  and  $\approx 620$  K, respectively. This increase of  $T_C$  is in line with reported experimental results [33,57]. However, at a medium Si concentration, the trend shifts to maintaining a constant  $T_C$  value within the range of 500–520 K for the experimental results and 630–670 K for the theoretical calculations. Conversely, high Si contents result in a decline in  $T_C$  with increasing Co amount. For instance, while  $\text{Fe}_{1.8}\text{Co}_{0.2}\text{P}_{0.6}\text{Si}_{0.4}$  exhibits a  $T_C$  of at  $\approx 640$  K, the  $T_C$  reduces to  $\approx 510$  K for  $\text{Fe}_{1.0}\text{Co}_{1.0}\text{P}_{0.6}\text{Si}_{0.4}$ . This trend is also evident in the theoretical results, where  $\text{Fe}_{1.8}\text{Co}_{0.2}\text{P}_{0.6}\text{Si}_{0.4}$  exhibits a  $T_C$  of  $\approx 780$  K, which declines to 710 K for  $\text{Fe}_{1.0}\text{Co}_{1.0}\text{P}_{0.6}\text{Si}_{0.4}$ .

These varied dependencies of  $T_C$  on Co concentration at different Si contents challenge conventional beliefs regarding the relationship between crystal structure and magnetic ordering temperature in compounds derived from  $\text{Fe}_2\text{P}$ . Typically, Curie temperatures increase as a result of a decrease in the  $c/a$  ratio. This general observation breaks down in the present series of  $\text{Fe}_{2-y}\text{Co}_y\text{P}_{1-x}\text{Si}_x$  as the  $c/a$  ratio systematically decreases with Co for Fe substitution (Fig. 5) while  $T_C$  may increase or decrease for low or high Si for P substitutions, respectively (Fig. 7).

The calculations for the preferential substitution sites for Co have shown no difference depending on the amount of

included Si. Therefore, the preferential sites cannot account for the disparate trends observed in  $T_C$ . This necessitates further investigation of the exchange interaction energies  $J_{ij}$  to identify the underlying reason.

#### H. Investigation of $J_{ij}$ energies for high and low Si and Co content

The exchange interaction energies in  $\text{Fe}_2\text{P}$  can be categorized into three distinct categories:  $3f$ - $3f$ ,  $3g$ - $3g$ , and  $3f$ - $3g$  contributions. The  $3f$ - $3f$  and  $3g$ - $3g$  exchange interactions can be further divided into intra- and interlayer exchange interaction energies [52]. Interlayer interactions occur between atoms in different layers on the  $c$  axis, while the intralayer interactions involve atoms within the same layer in the  $a$  or  $b$  directions. For this study, the Fe-P exchange interaction energies for  $\text{Fe}_2\text{P}$  were found to be negligibly small and therefore not further investigated.

Figure 8 illustrates the most significant contributions to the  $3f$ - $3f$ ,  $3f$ - $3g$ , and  $3g$ - $3g$  inter- and intralayer interaction energies as a function of Co content, for the  $\text{Fe}_{2-y}\text{Co}_y\text{P}_{1-x}\text{Si}_x$  ( $x = 0.1, 0.2,$  and  $0.4$  Si per f.u. and  $0 \leq y \leq 1$  Co per f.u.) compounds. The strongest interactions are the  $3g$ - $3g$  intralayer interactions, followed by the  $3f$ - $3g$  interlayer interactions and the  $3f$ - $3f$  intralayer interactions. The interlayer interactions are significantly weaker than the intralayer ones for both  $3f$ - $3f$  and  $3g$ - $3g$ . These results are in good agreement with previous theoretical studies [42,43,52].

At a fixed Co content (e.g., Co = 0.4), increasing Si substitutions lead to a general increase in the total interaction energy, in line with the observed systematic increase in Curie temperatures resulting from Si for P substitutions. Specifically, for the  $3f$ - $3f$  interaction energies [Fig. 8(a)] only minor changes ( $\sim 1$  meV) are observed on the intralayer interactions, whereas significant increases are observed for the interlayer exchange interaction energies.

The  $3f$ - $3g$  exchange interaction energies demonstrate a general increase of 1–2 meV from Si = 0.1 to 0.2 and an increase of 2–4 meV from Si = 0.2 to 0.4. Regarding  $3g$ - $3g$  interactions, a decrease of  $\sim 1$  meV is observed for the intralayer  $J_{ij}$ , while an increase of 1–2 meV is observed for the interlayer  $J_{ij}$ . Consequently, the total  $J_{ij}$  energy for  $3g$ - $3g$  interactions is only weakly affected by Si substitutions.

Overall, Si for P substitutions most significantly enhance the  $3f$ - $3g$  interaction. The pronounced contraction of the  $c$  axis upon Si for P substitutions is likely the main driver for this evolution by shrinking the distance between  $3f$  and  $3g$  metal layers. The evolution of the exchange interactions upon Si for P substitutions in  $\text{Fe}_{2-y}\text{Co}_y\text{P}_{1-x}\text{Si}_x$  quaternary compounds turns out to be qualitatively similar with former investigations in  $\text{Fe}_2\text{P}_{1-x}\text{Si}_x$  ternaries [43].

The impact of Co substitution on the  $J_{ij}$  energies has been systematically examined for the three Si contents: Si = 0.1, 0.2, and 0.4. For the intralayer  $3f$ - $3f$  interaction energies, at a fixed Si content (with the exception of the peculiar case Co = 1), Co substitution for Fe progressively strengthens the intralayer interaction while suppressing the interlayer one. Most importantly, the extent of the decrease in the  $3f$ - $3g$  interlayer interaction is highly sensitive to the Si content.



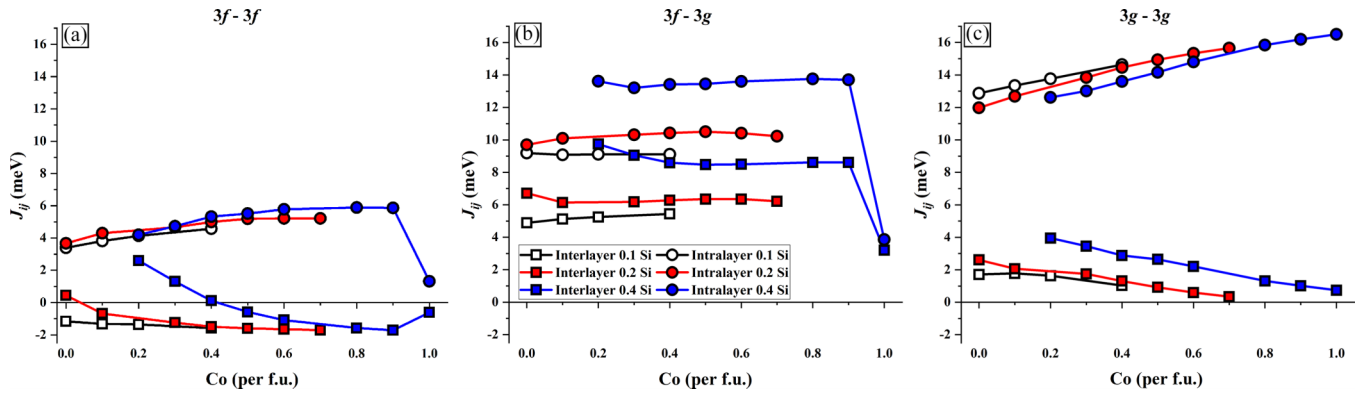


FIG. 8. Calculated (a) 3f-3f, (b) 3f-3g, and (c) 3g-3g inter- and intralayer interaction energies  $J_{ij}$  dependent on the Co amount for  $y = 0.1, 0.2,$  and  $0.4$  Si per f.u.

For the Si = 0.1 compound, the 3f-3f interlayer energy slowly decreases from negative  $\sim -1$  meV for Co = 0 down to  $\sim -1.5$  meV for Co = 0.4. Whereas for Si = 0.4, the 3f-3f interlayer energy is strongly suppressed from positive  $\sim 2.5$  meV for Co = 0.2 down to negative  $\sim -1.5$  meV at 0.8–0.9 Co per f.u. At 1.0 Co per f.u., the peculiar case of a complete occupancy of the 3f site by Co is reached. It results in a slight increase in the interlayer 3f-3f interaction once more, which can be attributed to the complete substitution of the Fe-3f site with Co.

Co substitutions for Fe do not significantly affect the 3f-3g exchange interaction energies. In all three cases of Si content, these energies fluctuate within a narrow range. The only noticeable effect of Co substitution occurs at 1.0 Co per f.u., where, similar to the 3f-3f interlayer interactions, the exchange nearly collapses due to the complete occupation of the 3f sites with Co.

When comparing the 3g-3g exchange interactions, an increase in the intralayer interactions and a decrease in the interlayer interactions with increasing Co content are observed, as shown in Fig. 8(c). The relatively parallel nature of the values indicates that the impact of Co on different Si contents is minimal. The substitution of Co for Fe occurs exclusively in the Fe-3f site, with only an indirect influence on the 3g sites. The contraction of the  $a$  axis strengthens the intralayer interaction, while the expansion of the  $c$  axis suppresses the interlayer interaction. These opposing changes nearly compensate for each other, resulting in a minimal overall effect on the total 3g-3g interaction.

The most significant evolution due to Co for Fe substitutions is observed on the 3f-3f interlayer energies, which are critically dependent on the Si content. This suggests that these interaction energies are the primary cause of the varying trends in  $T_C$  upon Co substitutions. At the Si content of 0.1, the 3f-3f interlayer energies exhibit only a slight decrease, which is compensated by an increase of the intralayer ones. However, as the Si content increases the decrease becomes more pronounced, potentially explaining the observed stability of  $T_C$  at medium Si concentrations. High Si contents (Si = 0.4) introduce a significant positive 3f-3f interlayer exchange, but Co for Fe substitutions quickly cause its collapse, resulting in a decreased total exchange energy and a consequent decrease in  $T_C$ .

Our results demonstrate a high sensitivity of the magnetism of the 3f site to chemical substitutions in  $\text{Fe}_{2-y}\text{Co}_y\text{P}_{1-x}\text{Si}_x$  quaternary compounds. This finding aligns with the “mixed-magnetism” scenario developed to account for the first-order magnetic transition observed in the parent  $\text{Fe}_2\text{P}$  or in  $\text{MnFe}(\text{P},\text{Si})$  magnetocaloric compounds [37,41,65–67]. Previous studies have highlighted the distinct behaviors of the 3g site, which carries high magnetic moments with robust exchange interactions, and the 3f site, which has weaker magnetic moments and interactions which are actually at the edge of stability in the  $\text{Fe}_2\text{P}$  parent. In the  $\text{Fe}_{2-y}\text{Co}_y\text{P}_{1-x}\text{Si}_x$  quaternary compounds, Si for P substitutions increase the magnetic moments and strengthen the interactions at the 3f site, thereby enhancing the overall ferromagnetism. Conversely, Co for Fe substitutions have the opposite effect, weakening the magnetism of the 3f site.

#### IV. CONCLUSION

This work investigates the effect of Si and Co substitution on  $\text{Fe}_2\text{P}$ , including the ternary  $\text{Fe}_2\text{P}_{1-x}\text{Si}_x$  and quaternary  $\text{Fe}_{2-y}\text{Co}_y\text{P}_{1-x}\text{Si}_x$  compounds, using both *ab initio* calculations and experimental methods. Special attention has been paid to the Curie temperature, with detailed analysis of the resulting trends based on Si and Co substitutions through the calculation of exchange interaction energies  $J_{ij}$ .

Phase transition investigations revealed experimental transitions at 0.1 or 0.25 Si per f.u. from the hexagonal to the BCO crystal structure, and further to a transition into a mixed-phase region at  $x \approx 0.5$  Si per f.u. Theoretical findings of a transition at  $\sim 0.1$  and  $0.6$  Si per f.u. aligned with the low temperature data and an assumed temperature dependency [19,20,33]. Further calculations on the substitution sites revealed that the  $2c$  site is likely to be preferred for Si substitution, while the 3f site is preferred for Co substitution. However, this leads in the case of Si to an increase in the formation energy and to a decrease in the case of Co.

The methodology employed in this study successfully reproduced the experimentally observed trends of higher magnetic moments and, consequently, higher saturation polarization and  $|BH|_{\text{max}}$ . The calculated magnetic moment has been found to be  $3.64 \mu_B/\text{f.u.}$ , higher than the experimental value of  $3.16 \mu_B/\text{f.u.}$  for the ternary  $\text{Fe}_2\text{P}_{0.5}\text{Si}_{0.5}$

compound. For Co substitution, a downward trend in magnetic moments was observed in both  $\text{Fe}_{2-y}\text{Co}_y\text{P}_{0.84}\text{Si}_{0.16}$  and  $\text{Fe}_{2-y}\text{Co}_y\text{P}_{0.59}\text{Si}_{0.41}$ , reducing the magnetic moments to 2.30 and 2.49  $\mu_B/\text{f.u.}$ , respectively.

The MFA consistently overestimates  $T_C$  in the FM state but agrees with the trends of the experimental data. In addition to the general increase in the  $T_C$  with Si, three different trends for Co substitution were identified. For low Si contents an improvement of  $T_C$  with more Co was found. Medium concentrations of Si resulted in consistent Curie temperatures, while high Si amounts, however, led to decreasing  $T_C$  with increasing Co.

A detailed analysis of the exchange interaction energies identified the Fe 3*f*-3*f* interlayer exchange interaction energies as the most likely reason for the different  $T_C$  trends, as they are changing drastically depending on the amount

of Si. Further studies on ternary  $\text{Fe}_2(\text{P,Si})$  single crystals and quaternary  $(\text{Fe,Co})_2(\text{P,Si})$  compounds are needed to deeply understand the underlying reasons for the influence of each element on the magnetic and structural properties. Additionally, theoretical investigations on phase stabilities, as well as magnetocrystalline anisotropy would further advance the understanding of these ternary and quaternary compounds.

## ACKNOWLEDGMENTS

The simulations were performed at the HPC Cluster ROSA, located at the University of Oldenburg (Germany) and funded by the DFG through its Major Research Instrumentation Programme (INST 184/225-1 FUGG) and the Ministry of Science and Culture (MWK) of the Lower Saxony State.

- 
- [1] S. Erdmann, T. Klüner, and H. İ. Sözen, *J. Magn. Magn. Mater.* **572**, 170645 (2023).
- [2] H. İ. Sözen and T. Klüner, *J. Magn. Magn. Mater.* **559**, 169529 (2022).
- [3] H. İ. Sözen, S. Ener, F. Maccari, K. P. Skokov, O. Gutfleisch, F. Körmann, J. Neugebauer, and T. Hickel, *Phys. Rev. Mater.* **3**, 084407 (2019).
- [4] H. İ. Sözen, S. Ener, F. Maccari, B. Fayyazi, O. Gutfleisch, J. Neugebauer, and T. Hickel, *Phys. Rev. Mater.* **7**, 014410 (2023).
- [5] T. Wittemann, H. İ. Sözen, M. Oezaslan, and T. Klüner, *Z. Naturforsch. B* **79**, 177 (2024).
- [6] J. M. Coey, *Engineering* **6**, 119 (2020).
- [7] Directorate-General for Internal Market, Industry and SMEs (European Commission), M. Grohol, and C. Veeh, Study on the Critical Raw Materials for the EU 2023 – Final Report, Luxembourg Publications Office of the European Union, 2023.
- [8] D. Bauer, D. Diamond, J. Li, M. McKittrick, D. Sandalow, and P. Telleen, U.S. Department of Energy, Office of Policy and International Affairs, 1 (2011), [https://www.energy.gov/sites/default/files/2019/06/f63/DOE\\_CMS2011\\_FINAL\\_Full\\_1.pdf](https://www.energy.gov/sites/default/files/2019/06/f63/DOE_CMS2011_FINAL_Full_1.pdf).
- [9] EU Ad-Hoc Working Group on Raw Materials, Report on Critical Raw Materials for the EU (2014), <https://ec.europa.eu/docsroom/documents/10010/attachments/1/translations/en/renditions/pdf>.
- [10] T. G. Woodcock, Y. Zhang, G. Hrkac, G. Ciuta, N. M. Dempsey, T. Schrefl, O. Gutfleisch, and D. Givord, *Scr. Mater.* **67**, 536 (2012).
- [11] Y. He, P. Adler, S. Schneider, I. Soldatov, Q. Mu, H. Borrmann, W. Schnelle, R. Schaefer, B. Rellinghaus, G. H. Fecher, and C. Felser, *Adv. Funct. Mater.* **32**, 2107513 (2022).
- [12] H. Fujii, T. Hokabe, T. Kamigaichi, and T. Okamoto, *J. Phys. Soc. Jpn.* **43**, 41 (1977).
- [13] L. Häggström, L. Severin, and Y. Andersson, *Hyperfine Interact.* **94**, 2075 (1994).
- [14] L. Caron, M. Hudl, V. Höglin, N. H. Dung, C. P. Gomez, M. Sahlberg, E. Brück, Y. Andersson, and P. Nordblad, *Phys. Rev. B* **88**, 094440 (2013).
- [15] K. J. D. Vos, W. A. Velge, M. G. V. D. Steeg, and H. Zijlstra, *J. Appl. Phys.* **33**, 1320 (1962).
- [16] R. Wäppling, L. Häggström, T. Ericsson, S. Devanarayanan, E. Karlsson, B. Carlsson, and S. Rundqvist, *J. Solid State Chem.* **13**, 258 (1975).
- [17] L. Lundgren, G. Tarmohamed, O. Beckman, B. Carlsson, and S. Rundqvist, *Phys. Scr.* **17**, 39 (1978).
- [18] R. Fruchart, A. Roger, and J. P. Sénateur, *J. Appl. Phys.* **40**, 1250 (1969).
- [19] P. Jernberg, A. A. Yousif, L. Häggström, and Y. Andersson, *J. Solid State Chem.* **53**, 313 (1984).
- [20] L. Severin, L. Häggström, L. Nordström, Y. Andersson, and B. Johansson, *J. Phys.: Condens. Matter* **7**, 185 (1995).
- [21] G. Kresse and J. Furthmüller, *Phys. Rev. B* **54**, 11169 (1996).
- [22] G. Kresse and J. Furthmüller, *Comput. Mater. Sci.* **6**, 15 (1996).
- [23] J. P. Perdew, K. Burke, and M. Ernzerhof, *Phys. Rev. Lett.* **77**, 3865 (1996).
- [24] A. Liechtenstein, M. Katsnelson, V. Antropov, and V. Gubanov, *J. Magn. Magn. Mater.* **67**, 65 (1987).
- [25] J. Koringa, *Physica* **13** 392 (1947).
- [26] W. Kohn and N. Rostoker, *Phys. Rev.* **94**, 1111 (1954).
- [27] H. Akai, <http://kkri.issp.u-tokyo.ac.jp>.
- [28] H. Shiba, *Prog. Theor. Phys.* **46**, 77 (1971).
- [29] H. Akai, *Physica B+C* **86–88**, 539 (1977).
- [30] P. Hohenberg and W. Kohn, *Phys. Rev.* **136**, B864 (1964).
- [31] W. Kohn and L. Sham, *Phys. Rev.* **140**, A1133 (1965).
- [32] V. L. Moruzzi, J. F. Janak, and A. R. Williams, *Calculated Properties of Metals* (Pergamon, New York, 1978).
- [33] L. L. Bao, H. Yibole, J. Y. Xu, Z. Q. Ou, O. Haschuluu, O. Tegus, N. H. van Dijk, E. Brück, and F. Guillou, *J. Alloys Compd.* **903**, 163770 (2022).
- [34] A. Nylund, A. Roger, J. P. Sénateur, and R. Fruchard, *J. Solid State Chem.* **4**, 115 (1972).
- [35] X. F. Miao, L. Caron, P. Roy, N. H. Dung, L. Zhang, W. A. Kockelmann, R. A. de Groot, N. H. van Dijk, and E. Brück, *Phys. Rev. B* **89**, 174429 (2014).
- [36] M. Bacmann, J.-L. Soubeyroux, R. Barrett, D. Fruchart, R. Zach, S. Niziol, and R. Fruchart, *J. Magn. Magn. Mater.* **134**, 59 (1994).
- [37] N. H. Dung, L. Zhang, Z. Q. Ou, L. Zhao, L. van Eijck, A. M. Mulders, M. Avdeev, E. Suard, N. H. van Dijk, and E. Brück, *Phys. Rev. B* **86**, 045134 (2012).

- [38] J. C. Slater, *J. Chem. Phys.* **41**, 3199 (1964).
- [39] N. E. Sagatov, P. N. Gavryushkin, M. V. Banayev, T. M. Inerbaev, and K. D. Litasov, *High Press. Res.* **40**, 235 (2020).
- [40] Z. Yang, S. Wu, X. Zhao, M. C. Nguyen, S. Yu, T. Wen, L. Tang, F. Li, K. M. Ho, and C. Z. Wang, *J. Appl. Phys.* **124**, 073901 (2018).
- [41] Z. Gercsi, E. K. Delczeg-Czirjak, L. Vitos, A. S. Wills, A. Daoud-Aladine, and K. G. Sandeman, *Phys. Rev. B* **88**, 024417 (2013).
- [42] I. A. Zhuravlev, V. P. Antropov, A. Vishina, M. van Schilfhaarde, and K. D. Belashchenko, *Phys. Rev. Mater.* **1**, 051401(R) (2017).
- [43] E. K. Delczeg-Czirjak, Z. Gercsi, L. Bergqvist, O. Eriksson, L. Szunyogh, P. Nordblad, B. Johansson, and L. Vitos, *Phys. Rev. B* **85**, 224435 (2012).
- [44] A. Catalano, R. J. Arnott, and A. Wold, *J. Solid State Chem.* **7**, 262 (1973).
- [45] B. Malaman, G. L. Caër, P. Delcroix, D. Fruchart, M. Bacmann, and R. Fruchart, *J. Phys.: Condens. Matter* **8**, 8653 (1996).
- [46] R. Chandra, S. Bjarman, T. Ericsson, L. Häggström, C. Wilkinson, R. Wäppling, Y. Andersson, and S. Rundqvist, *J. Solid State Chem.* **34**, 389 (1980).
- [47] X. F. Miao, N. V. Thang, L. Caron, H. Yibole, R. I. Smith, N. H. van Dijk, and E. Brück, *Scr. Mater.* **124**, 129 (2016).
- [48] E. K. Delczeg-Czirjak, L. Delczeg, M. P. J. Punkkinen, B. Johansson, O. Eriksson, and L. Vitos, *Phys. Rev. B* **82**, 085103 (2010).
- [49] S. K. Jain, S. Kumar, P. S. Krishna, A. B. Shinde, A. Krishnamurthy, and B. K. Srivastava, *J. Alloys Compd.* **439**, 13 (2007).
- [50] X. F. Miao, S. Y. Hu, F. Xu, and E. Brück, *Rare Metals* **37**, 723 (2018).
- [51] E. K. Delczeg-Czirjak, L. Bergqvist, O. Eriksson, Z. Gercsi, P. Nordblad, L. Szunyogh, B. Johansson, and L. Vitos, *Phys. Rev. B* **86**, 045126 (2012).
- [52] X. B. Liu, J. P. Liu, Q. Zhang, and Z. Altounian, *Phys. Lett. A* **377**, 731 (2013).
- [53] O. Eriksson, J. Sjöström, B. Johansson, L. Häggström, and H. Skriver, *J. Magn. Magn. Mater.* **74**, 347 (1988).
- [54] D. Zhu, T. Zhou, Q. Sun, and B. Shao, *J. Magn. Magn. Mater.* **587**, 171348 (2023).
- [55] S. Ishida, S. Asano, and J. Ishida, *J. Phys. F: Met. Phys.* **17**, 475 (1987).
- [56] H. Yibole, B. Lingling-Bao, J. Y. Xu, H. Alata, O. Tegus, W. Hanggai, N. H. van Dijk, E. Brück, and F. Guillou, *Acta Mater.* **221**, 117388 (2021).
- [57] S. Kumar, A. Krishnamurthy, and B. K. Srivastava, *Solid State Phenom.* **171**, 93 (2011).
- [58] L. H. Lewis and F. Jiménez-Villacorta, *Metall. Mater. Trans. A* **44**, 2 (2013).
- [59] J. M. Coey, *IEEE Trans. Magn.* **47**, 4671 (2011).
- [60] J. Y. Xu, Lingling-Bao, H. Yibole, and F. Guillou, *Solid State Commun.* **319**, 113996 (2020).
- [61] N. T. Trung, Z. Q. Ou, T. J. Gortenmulder, O. Tegus, K. H. Buschow, and E. Brück, *Appl. Phys. Lett.* **94**, 102513 (2009).
- [62] N. H. Long and H. Akai, *J. Phys.: Condens. Matter* **19**, 365232 (2007).
- [63] S. Köhler, G. Ruocco, and W. Schirmacher, *Phys. Rev. B* **88**, 064203 (2013).
- [64] D. A. Rowlands, *Rep. Prog. Phys.* **72**, 086501 (2009).
- [65] H. Yamada and K. Terao, *Phase Transitions* **75**, 231 (2002).
- [66] N. H. Dung, Z. Q. Ou, L. Caron, L. Zhang, D. T. Thanh, G. A. D. Wijs, R. A. D. Groot, K. H. Buschow, and E. Brück, *Adv. Energy Mater.* **1**, 1215 (2011).
- [67] E. K. Delczeg-Czirjak, M. Pereiro, L. Bergqvist, Y. O. Kvashnin, I. Di Marco, G. Li, L. Vitos, and O. Eriksson, *Phys. Rev. B* **90**, 214436 (2014).